Protein Science (1998), 7:358–368. Cambridge University Press. Printed in the USA.

A folding pathway for βpep-4 peptide 33mer: From unfolded monomers and β-sheet sandwich dimers to well-structured tetramers

KEVIN H. MAYO AND ELENA ILYINA

Department of Biochemistry, Biomedical Engineering Center, University of Minnesota, 420 Delaware Street, S.E., Minneapolis, Minnesota 55455

Abstract

It was recently reported that a de novo designed peptide 33mer, βpep-4, can form well-structured β-sheet sandwich tetramers (Ilyina E, Roongta V, Mayo KH, 1997b, *Biochemistry 36*:5245–5250). For insight into the pathway of βpep-4 folding, the present study investigates the concentration dependence of βpep-4 self-association by using ^{1}H-NMR pulsed-field gradient (PFG)-NMR diffusion measurements, and circular dichroism. Downfield chemically shifted αH resonances, found to arise only from the well-structured βpep-4 tetramer state, yield the fraction of tetramer within the oligomer equilibrium distribution. PFG–NMR-derived diffusion coefficients, *D*, provide a means for deriving the contribution of monomer and other oligomer states to this distribution. These data indicate that tetramer is the highest oligomer state formed, and that inclusion of monomer and dimer states in the oligomer distribution is sufficient to explain the concentration dependence of *D* values for βpep-4. Equilibrium constants calculated from these distributions [2.5×10^5 M^{-1} for M-D and 1.2×10^4 M^{-1} for D-T at 313 K] decrease only slightly, if at all, with decreasing temperature indicating a hydrophobically mediated, entropy-driven association/folding process. Conformational analyses using NMR and CD provide a picture where "random coil" monomers associate to form molten globule-like β-sheet sandwich dimers that further associate and fold as well-structured tetramers. βpep-4 folding is thermodynamically linked to self-association. As with folding of single-chain polypeptides, the final folding step to well-structured tetramer βpep-4 is rate limiting.

Keywords: β-sheet conformation; CD; folding; NMR; peptide; self-association

βpep peptides are de novo designed, water soluble, β-sheet–forming peptide 33mers (Mayo et al., 1996). Although other β-sheet–forming peptides have been designed to remain monomeric [β-hairpins (Blanco et al., 1993; Ramirez-Alvarado et al., 1996; de Alba et al., 1997)] or to form β-sheet sandwich dimers [betabellins (Richardson & Richardson, 1989; Richardson et al., 1992; Yan & Erickson, 1994) and betadoublet (Quinn et al., 1994)], βpep peptides self-associate primarily as tetramers at concentrations greater than a few mg/mL. βpep peptides, betabellins and betadoublets, have a similar number of amino acid residues (31 to 33) and are highly hydrophobic amphipaths—designed to self-associate through their hydrophobic faces. In these peptides, β-sheet formation is linked to the self-association process. β-Hairpins, on the other hand, are considerably shorter, less hydrophobic, and break the amphipathic scheme by avoiding the sequential pattern of alternating hydrophobic–hydrophilic residues (Richardson et al., 1992).

In most of these β-sheet–forming peptides compact structure is lacking, and transient β-sheet conformation is characterized by a strong CD band at 217 nm and a more "random coil" NMR spectrum (Mayo et al., 1996). βpep-4 is an exception, and forms well-structured β-sheet sandwich tetramers that are comprised of monomer subunits, each having the same three-stranded anti-parallel β-sheet fold (Ilyina et al., 1997a, 1997b). Two distinct dimer folds (called D1 and D2), however, are observed. In both dimer types, the N-terminal strand from one monomer associates with that from another in an anti-parallel fashion thereby continuing the β-sheet to six strands. Dimers differ at the monomer–monomer interface primarily by a two-residue shift in the alignment of β-strands. In the tetramer, dimers interact via the hydrophobic faces of their amphipathic structures. Current evidence suggests that heterotetramers comprised of dimers D1 and D2 form, as opposed to two types of homotetramers, each having D1 or D2 dimers.

The present study investigates the mechanism of βpep-4 folding from monomer to the final well-structured tetramer state. Questions

Reprint requests to: K.H. Mayo, Department of Biochemistry, University of Minnesota, 435 Delaware Street, S.E., Minneapolis, Minnesota 55455; e-mail: mayox001@maroon.tc.umn.edu.

Abbreviations: NMR, nuclear magnetic resonance; 2D-NMR, two-dimensional NMR spectroscopy; HOHAHA, 2D-NMR homonuclear Hartman-Hahn spectroscopy; NOE, nuclear Overhauser effect; NOESY, 2D-NMR nuclear Overhauser effect spectroscopy; PFG, pulsed field gradient; rf, radio frequency; FID, free induction decay; CD, circular dichroism; M, monomer; D, dimer; T, tetramer.

arise as to how much β-sheet folding occurs in the monomer state of βpep-4, do dimers exist to any great extent in solution, and how do fractional populations of oligomers vary with concentration and temperature? These and other related questions address the problem of designing sequences that can form β-sheet structure in the monomer state or perhaps better control formation of a desired oligomer state. The present NMR and CD study, therefore, is focused on analyzing βpep-4 under conditions where monomer and lower oligomer states are prevalent, i.e., low peptide concentration. Pulsed-field gradient (PFG) NMR self-diffusion measurements provide information on changes in the oligomer distribution as the βpep-4 concentration is varied. This information allows derivation of fractional oligomer populations and equilibrium constants. It is found that monomers, dimers, and tetramers alone can account for the concentration dependence in diffusion data. NMR and CD data acquired at low peptide concentrations indicate that monomers have mostly "random coil" conformation, while dimers appear to be molten globule-like, β-sheet sandwichs, which associate to form well-structured tetramers. The final folding step occurs on the slow chemical shift time scale (Jaenicke, 1991) and is rate limiting, as usually observed with the folding of single-chain polypeptides.

Results

Distribution of oligomer states

Figure 1 shows ^{1}H-NMR spectra acquired in D_2O at 283 and 313 K as a function of βpep-4 concentration. Downfield-shifted αH resonances result from formation of well-folded β-sheet sandwich tetramers (Mayo et al., 1996; Ilyina et al., 1997a, 1997b). As the βpep-4 peptide concentration is lowered at either temperature (Fig. 1), the downfield αH resonance area is decreased relative to the constant aromatic resonance area. This observation is consistent with tetramer dissociation. Although the concentration-dependent effect is expected, the pathway for the association/dissociation process is unknown.

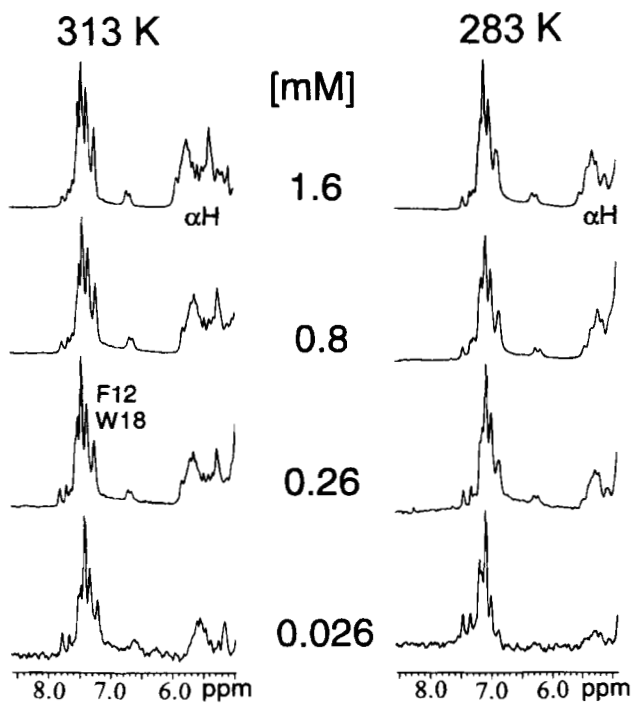

Fig. 1. NMR spectra for βpep-4. ^{1}H-NMR (600 MHz) spectra are shown for βpep-4 peptide in D_2O (pH 6) as a function of concentration (mM) as indicated in the figure. Series of spectra are shown for two temperatures, 283 and 313 K. Spectra were accumulated with 8 k data points over 6,000 Hz sweep width and were processed with 2 Hz line broadening. Only the spectral region downfield from the HDO resonance is shown.

The fraction of tetramer (T), f_T, in this equilibrium distribution can be calculated from the area under the downfield-shifted αH resonance envelope by calibrating it against the constant aromatic resonance area. From TOCSY spectra, the number of protons resonating within the most downfield part of this αH resonance envelope is 15 (Ilyina et al., 1997b). Using the cut and weigh method, the aromatic resonance area (Fig. 1) [10 protons from one phenylalanine (F12) and one tryptophan (W18)] yields a mass per proton. The ratio of the mass of the αH resonance envelope actually cut and weighed to that expected for the 15 proton αH resonance area, yields f_T. In some cases, numerical integration was used and results were, within error, the same. The cut-and-weigh method was easier to use, particularly in instances where baseline corrections near the HDO resonance were problematic. Table 1 lists f_T for temperatures and concentrations investigated. f_T varies from 0.9 at 5.3 mM to 0.15 at 0.026 mM at 313 K, and decreases with decreasing temperature. This "cold melt" results from the predominance of hydrophobic stabilizing forces (Tanford, 1981) within the βpep-4 tetramer. Plotting log [T conc.] vs. log [remainder conc.] yields a Hill plot with a slope of 1.9 to 2.2, indicating that tetramers dissociate primarily into dimers.

Sedimentation equilibrium ultracentrifugation is a commonly employed method used to derive fractional populations of oligomers in solution. For βpep-4, which undergoes rapid oligomer exchange, however, PFG NMR provides an easier and perhaps more informative way to derive average diffusion coefficients as a function of peptide concentration, which, in combination with other data described below, can yield fractional populations of oligomer species. Figure 2 plots PFG NMR-derived diffusion coefficients vs. βpep-4 concentration. Diffusion coefficients, D, have been measured at 278, 283, 288, 293, 303, and 313 K. Only D values acquired at 283 and 313 K are plotted in Figure 2. As described in Methods, D values normally were derived from the gradient-induced signal loss of upfield methyl and methylene resonances (average of three resonances). However, using the downfield-shifted αH resonances to determine D at either temperature results in a concentration-independent behavior, as plotted in Figure 2 (labeled αH). At 313 K, a D value of 15.6×10^{-7} cm^2 s^{-1} results, which falls close to the value for tetrameric βpep-4 (16.5×10^{-7} cm^2 s^{-1}) calculated from D values of standard folded proteins ribonuclease, lysozyme, and ubiquitin, using an exponent, a, of 1/3 for a compact globule in Equation 4 (see Methods). The slightly, but significantly lower D value may suggest that βpep-4 tetramers are somewhat more expanded (5 to 7%) than the protein standards. NOE data on tetramer βpep-4 indicate the presence of well-formed backbone to backbone contacts consistent with the presence of well-structured β-sheet dimers (Ilyina et al., 1997b); the tetramer sandwich, on the other hand, which is mediated by side chain-to-side chain interactions from the hydrophobic faces of amphipathic dimers, may be somewhat less compactly folded. Alternatively, this deviation could result from differences in shape. In any event, the observation confirms that downfield-shifted αHs are associated only with relatively well-folded βpep-4 tetramers and also provides an experimentally derived D value for the βpep-4 tetramer state.

Table 1. *Fraction of compact tetramer, f_T, calculated by using the cut and weigh method with αH and aromatic resonance envelopes as discussed in the text*[a]

mM	278 K	283 K	288 K	293 K	303 K	313 K
5.3	—	—	—	—	—	0.9
2.6	—	0.73	—	—	—	0.82
2.1	—	—	—	—	—	0.73
1.58	0.53	0.61	0.6	0.65	0.75	0.7
1.05	—	—	—	—	—	0.67
0.79	0.42	0.43	0.52	0.65	0.69	0.62
0.53	—	—	—	—	—	0.55
0.39	0.3	0.37	0.43	0.46	0.56	—
0.26	—	—	—	—	—	0.41
0.2	0.23	0.28	0.37	0.4	0.44	—
0.087	—	0.17	—	—	—	0.32
0.026	0.11	0.09	0.11	0.16	0.15	0.15

[a]The error in f_T is estimated to be ±0.03 for any given value. In this respect, lower f_T values have a greater percent error because both the tetramer population and the NMR spectral signal to noise (S/N) was lower. Errors can also arise from inaccuracies in determining the number of αH protons (estimated to be ±1 proton) within the cut αH resonance envelope.

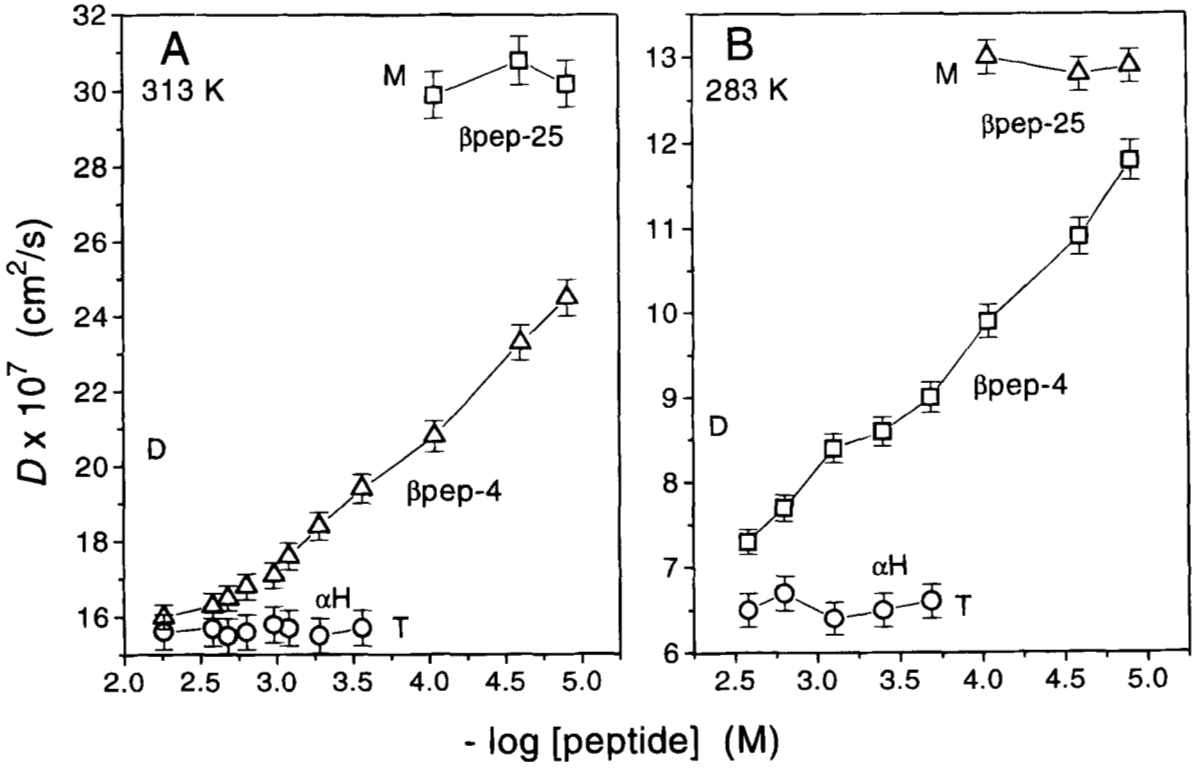

Fig. 2. PFG-derived diffusion coefficients for βpep-4. Pulsed-field gradient (PFG) NMR-derived diffusion coefficients have been determined as a function of peptide concentration for βpep-4 and for two its variants: βpep-25, which is monomeric at low peptide concentration, and an *N*-methyl derivative, which forms dimers as its highest aggregation state as discussed in the text. Each diffusion coefficient was determined from a series of 15 one-dimensional PFG spectra acquired using different g values. Experimental decay curves were approximated as single exponentials. Experimental conditions were: δ = 4 ms, g = 1 to 45 G/cm, Δ = 34.2 ms, and the longitudinal eddy-current delay T_e = 100 μs. The figure shows data acquired for two temperatures, 283 and 313 K. Data points (open symbols) represent the average of D values derived from the three different resonances used to measure them; error bars represent standard deviations from the average value.

D values measured at upfield resonances, on the other hand, vary considerably with changes in βpep-4 concentration and represent a weighted average over the equilibrium distribution of βpep-4 oligomer states, including tetramers. The slope of the log signal intensity vs. the square of gradient strength is linear. Initially, it was expected that the slower exchange rate for tetramers might result in non-linear gradient-induced decay curves for mixes of tetramer and other oligomer species, but this was not observed. There are two apparent reasons for this. First, is that at concentrations where tetramer predominates, reasonable populations of monomers do not enter the distribution, and only tetramers and dimers (as will become clear later) are the major contributors. Second, the slope of the decay curve for dimers is only 1.4 times that of tetramers, and data were acquired only up to a gradient strength of 45 G/cm. For these reasons one would not necessarily observe non-linear slopes for mixes of dimer and tetramer states. TOCSY spectra were checked to assure that resonances chosen for diffusion analysis included all oligomer states. The three resonances chosen did, in fact, show decay slopes within 2% of each other. At the highest βpep-4 concentrations, *D* values (313 K) measured at these three upfield resonances begin to plateau off on approach to the *D* value for tetramer βpep-4 (Fig. 2A), indicating that tetramer βpep-4 is the highest oligomer state formed. Consequently, because f_T is known (Table 1), only lower aggregate states need to be considered when deriving fractional populations of oligomer states from the concentration dependence of diffusion coefficients.

To exemplify how fractional distributions were derived, consider data acquired at 313 K (Fig. 2A). For βpep-4, D_T is 15.6×10^{-7} cm^2 s^{-1}. D_M and D_D, however, are unknown. Because different oligomer states exhibit various degrees of folding, D_M and D_D could not be derived with any accuracy by using D_T and Equation 4 (see Materials and methods), which is only valid when estimating relative sizes for groups of proteins that are either all compact ($a = 1/3$) or all random coil ($a = 1/2$). As will be evident below, lower oligomer states are considerably less structured than tetramer βpep-4. D_M could have been derived if the observed *D* value plateaued off at low βpep-4 concentrations, but this does not occur due to the relative stability of βpep-4 oligomers. For a nearly sequentially identical peptide 33mer, βpep-25: ANIKLSVQMKLF KRHLKWKIIVKLNDGRELSLD, however, oligomer stability is greatly reduced and at low peptide concentrations *D* values do plateau off as shown in Figure 2. At 313 K, the average of these three *D* values is 30.4×10^{-7} cm^2 s^{-1}, which falls within the range expected for monomer βpep-4 and, therefore, was used as D_M for βpep-4. At 283 K, the observed *D* value for βpep-4 does approach this value for D_M. To determine D_D, a variant of βpep-4 was synthesized with *N*-methyl at V7 (*N*-CH_3 variant) to prevent β-sheet–mediated dimer (and, therefore, tetramer) formation due to methyl group-induced steric hinderance between interfacial β-strands and to the inability of interfacial inter-strand NH hydrogen bonds to form (Rajarathnam et al., 1994, 1995). At higher concentrations, this βpep-4 *N*-CH_3 variant does demonstrate concentration-independent *D* values that fall in the range expected for dimer βpep-4 (Fig. 2). An average *D* value of 20.7×10^{-7} cm^2 s^{-1} (average *D* from four concentration points) was used as D_D for βpep-4.

At 313 K and 1.6 mM, the observed *D* value (D_{OBS}) for βpep-4 (Fig. 2A) is 16.7×10^{-7} cm^2 s^{-1}. This is weighted according to the following equation:

$$D_{OBS} = f_M(30.4) + f_D(20.7) + f_T(15.6) \quad (1)$$

where f_M, f_D, and f_T are the fractions of monomer, dimer, and tetramer, respectively, and values in parentheses are their respective diffusion coefficients (D_M, D_D, D_T from above) understood to be $\times 10^{-7}$ cm^2 s^{-1}. In this analysis, only D and T oligomers were considered, because T is the highest oligomer state and two observations indicated the presence of dimers: Hill plot slope of about 2, indicating dissociation of T to D and *N*–CH_3 variant forms dimers with no evidence for trimers. Therefore, using values for f_T from Table 1 and the relationship $1 - f_T = f_M + f_D$, fractional populations f_M and f_D were estimated using diffusion data in Figure 2. For example, at 0.087 mM, D_{OBS} falls close to that of a dimer, and with $f_T = 0.32$ (Table 1), $f_M = 0.13$ and $f_D = 0.55$. Figure 2B shows diffusion data acquired at 283 K. Note that although *D* values are smaller due to the lower temperature, they do reflect greater dissociation resulting from the "cold melt." For the most part, M, D, and T states alone (Equation 1) are sufficient to explain observed diffusion data. However, this does not exclude the possibility that a relatively small fraction (less than about 0.05) of an additional oligomer state may be present.

Derived M, D, and T fractional populations for βpep-4 are plotted in Figure 3 (solid symbols) for data acquired at 283 and 313 K. To assess the accuracy of derived fractional populations, dimer, and tetramer equilibrium association constants, K_D and K_T, were calculated at each βpep-4 concentration point shown in Figure 3. For data acquired at 313 K, log $K_{D,T}$ vs. log [peptide] is plotted in the insert. Although some variance is apparent, the range is limited. At 313 K, the average value for K_D is 2.5×10^5 M^{-1} $\pm$ 1.8×10^5 M^{-1}, and the average value for K_T is 1.2×10^4 M^{-1} $\pm$ 0.6×10^4 M^{-1}. Lines plotted in Figures 3A and 3B represent M, D, and T fractional populations calculated using average K_D and K_T values. Note that actual data points fall on or very close to these lines. Varying D_D or D_M by as much as $\pm 1 \times 10^{-7}$ cm^2 s^{-1} has little effect on f_D or f_M, modifying them at most by 0.05. This change in fractional population has less of an effect on K_T than it does on K_D because f_T is independently derived and f_D remains between 0.2 and 0.7 over this concentration range. K_D is most affected when f_M is less than 0.1, but even then K_D can be more accurately defined under conditions where f_M is greater. Note again that fits to these data using average values for K_D and K_T are quite good, thus providing increased confidence in the analysis.

Similar data (not shown) have been acquired at 278, 288, 293, and 303 K. K_D remains fairly constant with temperature, whereas K_T drops to 4×10^3 M^{-1} $\pm$ 2×10^3 M^{-1} by 278 K. Two general observations can be made: (1) K_D is always larger than K_T, and (2) the temperature dependence in K_T and K_D is shallow or nill. In this respect, the free energy of dimer formation ($\Delta G_D = -RT \ln K_D$) is more negative than that for tetramer formation ($\Delta G_T = -RT \ln K_T$). The absence of a significant temperature dependence, especially in K_D, indicates a near-zero enthalpic contribution to the subunit association process, which in turn, means that these folding steps are primarily entropy driven. Such thermodynamic trends are consistent with hydrophobically mediated events (Ross & Subramanian, 1981; Tanford, 1981).

Conformational analysis

Even though βpep-4 is known to fold as a well-structured, β-sheet sandwich tetramer (Ilyina et al., 1997a, 1997b), information on the degree of folding of βpep-4 monomers and dimers is lacking. For insight into the nature of these conformational states, CD and

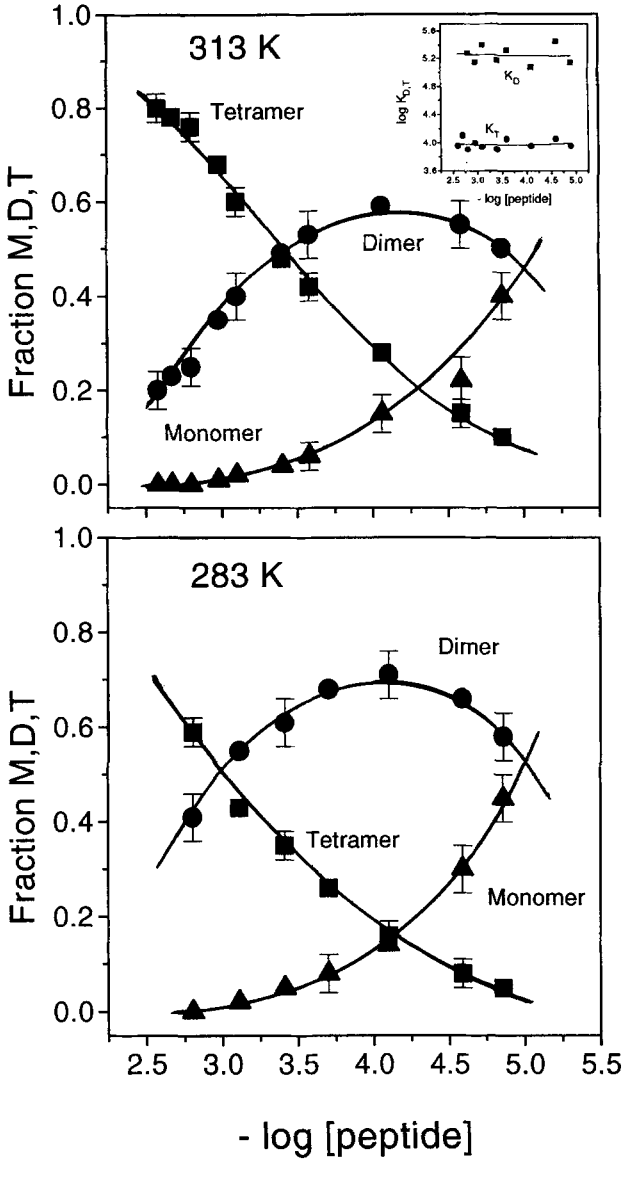

Fig. 3. Fractional populations for oligomer states. Fractional populations for monomer, dimer, and tetramer states, determined as described in the text, are plotted (filled-in symbols) versus the βpep-4 peptide concentration. Data are shown for two temperatures, 283 and 313 K. For f_T, error bars represent variations in using the cut and weigh method, whereas for f_M and f_D, error bars represent the range of values determined by recalculating fractional populations within the error limits for D values. Error bars are shown only for some data points. Lines drawn through experimental points represent fractional populations calculated from average values of K_D and K_T.

NMR spectra were acquired at low βpep-4 concentrations where tetramer populations are reduced and populations of dimer and monomer states are enhanced.

Analysis of diffusion data (Fig. 3) has indicated that at 313 K and 0.4 mM, βpep-4 dimers and tetramers are approximately equally populated (45–50%), and monomers are present at about 5%. Under these conditions, the CD trace (Fig. 4, left panel) shows a strong negative ellipticity centered at 217 nm. This CD band is characteristic of β-sheet conformation (Greenfield & Fasman, 1969; Johnson, 1990; Waterhous & Johnson, 1994). At 0.13 mM, where f_T has fallen to about 0.35 and f_D and f_M have risen to about 0.6 and near 0.1, respectively, the CD trace reflects mostly β-sheet structure with the appearance of a shoulder on the far UV side of the 217 nm band. Upon lowering the concentration further to 0.013 mM, f_T is less than 0.1, while f_D remains at about 0.6 and f_M rises to near 0.3. Here, CD data show an attenuated β-sheet band and a more prominent band between 200 and 205 nm, which is characteristic of random structure distributions predicted for mostly unstructured peptides (Bierzynski et al., 1982; Shoemaker et al., 1985; Waterhous & Johnson, 1994).

These results indicate that as the concentration is lowered and the monomer population is increased, the population of "unstructured" βpep-4 increases. The logical conclusion is that βpep-4 is more "unstructured" in the monomer state relative to that in dimer and tetramer states. This view is reinforced by analyzing CD spectra acquired at 0.013 mM and at the lower temperature of 278 K (Fig. 4, right panel), where monomer βpep-4 represents at least 80% of the oligomer species. Now, the CD trace more clearly shows that monomer βpep-4 is indeed mostly unstructured. A shoulder on the near-UV side of the main band appears to account for the 20% or so dimer (β-sheet) present. Present CD data also explain why earlier CD results on βpep-4 (Mayo et al., 1996) showed nearly equally intense CD bands at 204 nm and 217 nm. In that study, CD data were acquired using a peptide concentration of 0.11 mM [not the 10–20 mM as stated in the Figure 8 legend (erratum)]. At this concentration, and particularly at 278 K, considerable amounts of monomer βpep-4 are present in solution.

From the present study, it also may be concluded that βpep-4 dimers are comprised mostly of β-sheet structure because the 217 nm CD band is the more prominent at concentrations where mostly dimers or dimers and tetramers are present. Related to this is the question of whether dimer βpep-4 is well structured and compactly folded or not. Because only tetramer βpep-4 shows highly downfield-shifted αH resonances indicative of well-structured β-sheet conformation (Mayo et al., 1996; Ilyina et al., 1997a, 1997b), it is likely that dimer βpep-4 forms transient β-sheet conformation. For further insight into the conformational characteristics of the dimer state, 2D NMR TOCSY and NOESY spectra were acquired at concentrations of 0.32 and 0.079 mM to maximize the dimer population and reduce the tetramer population while still allowing for reasonable ^{1}H-NMR signal to noise. Because peptide concentrations were low and oligomer populations were spread primarily over dimer and tetramer states thereby lowering effective concentrations in each state, data were acquired only in D_2O in order to minimize problems with solvent suppression and to observe αH resonances close to the water resonance.

Figure 5 shows the αH region from TOCSY spectra acquired at 5.3 mM (313 K) (left panel), 0.079 mM (313 K) (middle panel), and 0.079 mM (283 K) (right panel). Downfield-shifted αH resonances assigned to residues which form the β-sheet in well-structured βpep-4 tetramers (Ilyina et al., 1997b) are labeled (left panel). At the highest peptide concentration where mostly tetramer βpep-4 is present, the more upfield αH resonances arise primarily from N-terminal and loop residues: S1, I2, Q3, R13, K14, Q15, A16, K17, N25, D26, G27, and R28, associated with the tetramer state. Some cross-peaks for these residues have also been labeled in Figure 5 (left panel). When the βpep-4 concentration is lowered to 0.32 mM, downfield αH cross-peak intensities are diminished while more upfield αH resonances are increased in intensity (data not shown). This results from an increase in dimer population and indicates, not unexpect-

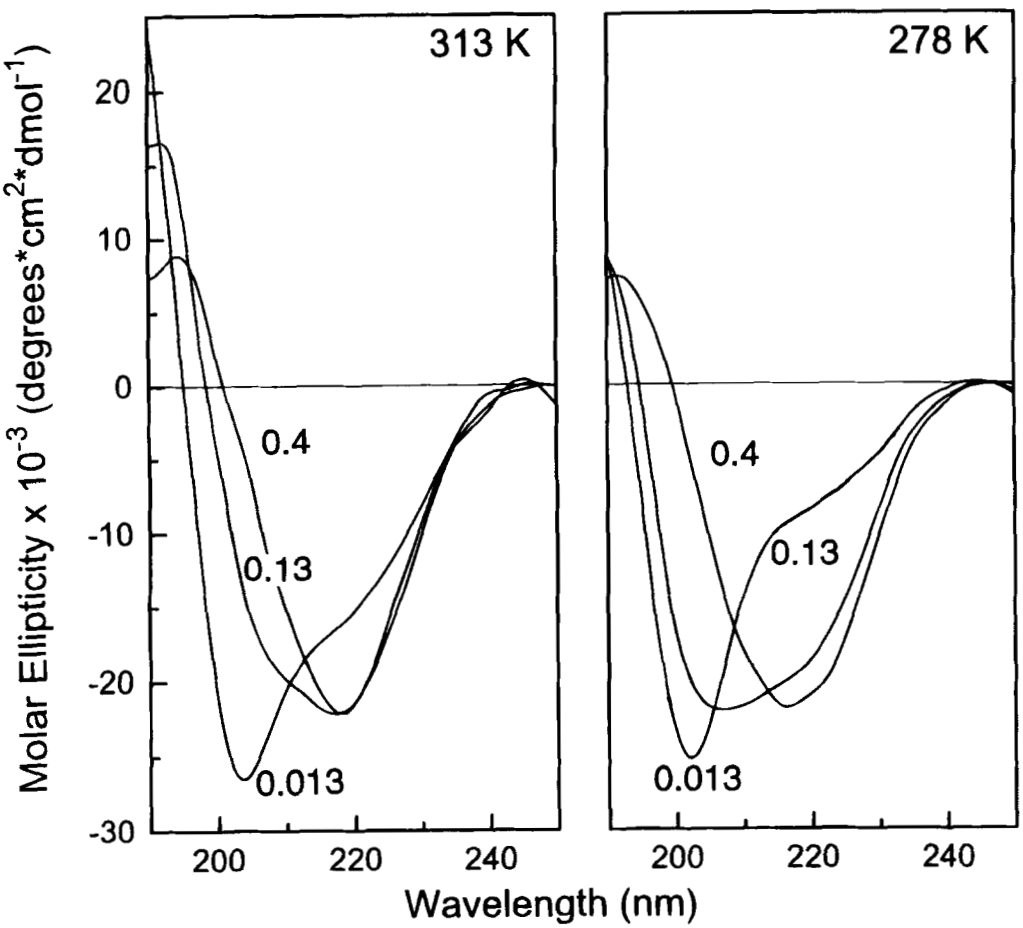

Fig. 4. CD Spectra of βpep-4. Far-ultraviolet circular dichroic spectra for βpep-4 peptide are shown as mean residue ellipticity versus wavelength (nm). Peptide concentration was varied from 0.013 mM to 0.4 mM, as indicated in the figure. The pH was adjusted to pH 6. Data for two temperatures are shown: 278 and 313 K. Other experimental variables are given in Materials and methods.

edly, that αH resonances in the dimer state overlap with N-terminal and loop αH resonances arising from the tetramer state. This trend is more pronounced at 0.079 mM (Fig. 5, middle panel), where the dimer population is about twice that of the tetramer and the monomer population is minimal. To further reduce the tetramer population at 0.079 mM, the temperature was lowered to 283 K, where dimer and monomer populations are about 70 and 10%, respectively. Now, TOCSY cross-peaks from mostly upfield αH resonances are apparent (Fig. 5, right panel). As noted earlier, some well-structured tetramer exists even under these conditions, as evidenced by the presence of downfield shifted αHs (observe diagonal). Resonance amplitudes for tetramers, however, are reduced and broadened due to chemical exchange at reduced tetramer populations. It is partly for this reason that TOCSY cross-peaks for the tetramer are very weak or are not observed. From this series of experiments it is not only evident which resonances are associated with lower oligomer states (primarily dimers), but confirms that resonances from the tetramer state are in slow chemical exchange (NMR chemical shift time scale) with resonances associated with those lower oligomer states.

NOESY spectra provided little additional information, and because data were not acquired in H_2O for reasons given above, the standard sequential assignment approach on the dimer state could not be used. However, a number of amino acid spin systems in the dimer state could be identified as labeled in Figure 5 (right panel). For example, βpep-4 has three serines, and three serine spin systems are observed. Using the Wishart et al. (1992) chemical shift index (labeled at the bottom of the middle panel in Figure 5), the most upfield of these αHs falls within the random coil chemical shift range, while the other two αHs resonate 0.13 and 0.21 ppm downfield from the random coil position. This suggests that two serines are involved in β-sheet conformation. For reference, Figure 6 shows the β-sheet fold in a monomer subunit from tetramer βpep-4 (Ilyina et al., 1997b). Note that S1 is N-terminal, while both S8 and S31 are indeed involved in β-sheet structure. Similar comparisons suggest that two or three [in particular W18 (distinguished by an NOE between its βH_2 and ring proton resonances)] of the seven AMX spin systems, one or two of the three Q/Es, the unique M9 [distinguished from Q/E spin systems by more downfield shifted βH_2 and γH_2 resonances (Wüthrich, 1986)], one of the two arginines [identified from δH_2–αH TOCSY cross-peaks], at least two of the five lysines, and it appears most of the β-branched hydrophobic residue αHs are also 0.1 to 0.3 ppm downfield shifted from their respective random coil positions. This fair number of downfield-shifted αHs indicates the presence of β-sheet conformation in the βpep-4 dimer state, which is consistent with CD data.

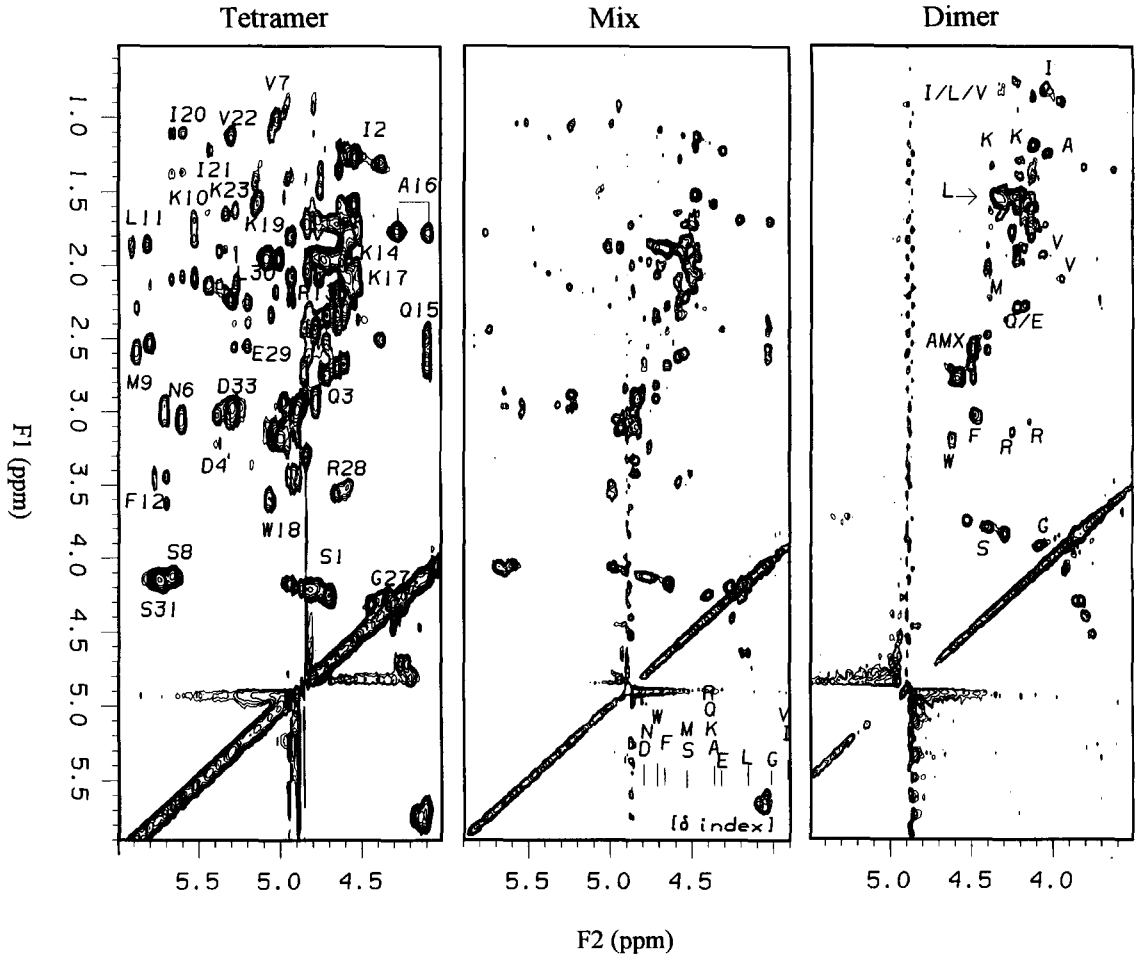

Fig. 5. HOHAHA Spectra for βpep-4. HOHAHA contour plots are shown for βpep-4 peptide in D_2O. Solution conditions were varied from 5.3 mM βpep-4, 313 K (left panel) to 0.079 mM βpep-4, 313 K (middle panel) to 0.079 mM βpep-4, 283 K (right panel). Two hundred fifty-six hypercomplex FIDs containing 2 k words each were collected and processed as discussed in Materials and methods. Data were zero-filled to 1024 in t1. The raw data were multiplied by a 30° shifted sine-squared function in t1 and t2 prior to Fourier transformation. Labeling of resonances is as discussed in the text.

By assuming that a particular αH chemical shift difference [tetramer–random coil (rc)] ($\Delta\delta_{T\text{-}rc}$) represents fully folded β-sheet, the percent β-sheet fold in the dimer can be estimated by taking the ratio of αH chemical shift differences: $[\Delta\delta_{D\text{-}rc}]/[\Delta\delta_{T\text{-}rc}] \times 100$. The average percentage of β-sheet fold in the dimer state is estimated to be between 30 and 35%, with a range of 26 to 48%, depending upon which αH resonance is used. This combined with the apparent absence of conformationally informative inter-strand NOEs, for example, αH-αH, suggests that the β-sheet structure within the dimer state is transient. The βpep-4 dimer exhibits characteristics of a molten globule (Jaenicke, 1991; Ptitsyn & Semisotnov, 1991) by possessing considerable β-sheet conformation with little, if any, fixed tertiary structure.

Because a high-resolution structure for dimer βpep-4 is naturally lacking, it is unknown if the β-strands and their alignments in the β-sheet are the same in the dimer as those in the well-folded tetramer (Fig. 6) (Ilyina et al., 1997b). Some insight into this can be derived from αH chemical shifts of βpep-4 dimer resonances described above. In the dimer, both valines, two serines, the methionine (M9), one arginine, at least two lysines, and most of the isoleucines and leucines appear to be involved in β-sheet structure. This distribution is similar to that in β-strands in a monomer subunit of the tetramer (Fig. 6). Moreover, the unique alanine, A16, which is positioned within a loop between β-strands 1 and 2 in a monomer subunit of the tetramer, exhibits a random coil αH chemical shift in the dimer, consistent with its not being part of a β-strand in the dimer. That loop sequence also contains two lysines, and in the dimer state, about two lysines do show random coil chemical shifts. Although this is by no means proof that the transient β-sheet fold in the dimer is the same as in the tetramer, it is suggestive.

Discussion

The data presented here suggest a pathway for the folding and unfolding of βpep-4 as summarized by the following equilibria:

$$M \Leftrightarrow D_{MG} \Leftrightarrow T_{(D1+D2)}. \quad (2)$$

Monomer (M) species are mostly composed of random coil structures with the possible presence of some partially folded, β-sheet

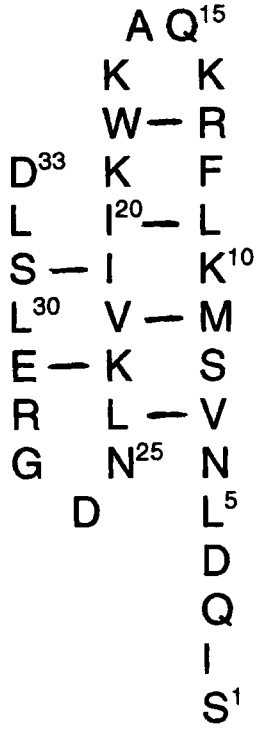

Fig. 6. Backbone fold for monomer βpep-4. The backbone fold for the monomer subunit from compact tetramer βpep-4 (Ilyina et al., 1997b) is shown. Lines connect inter-strand αH-αH groups in the anti-parallel β-sheet conformation.

structure. Monomers associate to form molten globule-like, β-sheet dimers (D_{MG}) with an equilibrium between the two, which is shifted to D_{MG}. Association of monomers into dimers could occur in two ways: (1) through the hydrophobic faces of amphipathic β-sheet monomers or (2) via continuation of the monomer anti-parallel β-sheet into a six-stranded structure like that found in well-structured βpep-4 tetramers (Ilyina et al., 1997). If the β-sheet were merely continued in D_{MG}, however, the hydrophobic surface of the amphipathic dimer would remain mostly exposed to solvent water, and this would be thermodynamically unfavorable and likely yield very small populations of D_{MG}. The fractional population of D_{MG} derived from the analysis of diffusion data, however, is rather large. Combined with the apparent temperature independence in K_D, which suggests hydrophobically mediated dimerization, i.e., negative ΔG, near zero ΔH and highly positive ΔS (Ross & Subramanian, 1981), the more probable way for monomers to associate is as β-sheet sandwich dimers. Perhaps the best evidence for formation of β-sheet sandwich dimers comes from the observation that the βpep-4 V7 *N*-methyl variant, which cannot form six-stranded β-sheet type dimers, still dimerizes. Betabellin (Richardson & Richardson, 1989; Richardson et al., 1992; Yan & Erickson, 1994) and betadoublet (Quinn et al., 1994) peptides also associate as β-sheet sandwich dimers. In the pathway shown above, βpep-4 D_{MG} then associate to form well-folded, β-sheet sandwich tetramers ($T_{(D1+D2)}$). Here, D_1 and D_2 represent the two types of six-stranded β-sheet dimers observed in the NMR-derived structure of βpep-4 tetramers (Ilyina et al., 1997b).

General aspects of the βpep-4 folding pathway are depicted in the free energy level diagram in Figure 7. Because K_D is greater that K_T, the free energy for formation of D_{MG} ($\Delta G_D^{313K} = -7.3$ kcal/mol) is greater than that for the D_{MG}-D_{MG} association step and transition to the well-structured tetramer ($\Delta G_T^{313K} = -5.7$ kcal/mol). The overall free energy for formation of well-structured tetramers is −20.3 kcal/mol ($2\Delta G_D + \Delta G_T$). Interestingly, this is almost the same value obtained for the free energy of formation of alpha 1 peptide into a tetramer four-helix bundle (−20.8 kcal/mol) (Kaumaya et al., 1990). Thermodynamic stabilities of other four-helix bundles (Munson et al., 1994; Bryson et al., 1995) and coiled coils (Harbury et al., 1993; Lumb et al., 1994; Zitzewitz et al., 1995) formed from similar length peptides or similar numbers of amino acid residues, are similar to free energies of association/folding for βpep-4. For examples, ΔG values are −8.1 kcal/mol, −7.3 kcal/mol, and −7.5 kcal/mol, respectively, for folding dimeric four-helix bundles Rop11, Rop13, and Rop21 (Munson et al., 1994); −7.8 kcal/mol for folding alpha 3, another dimeric four-helix bundle (Kaumaya et al., 1990), and −10.5 kcal/mol for folding the leucine zipper peptide 33mer GCN4-p1 (Zitzewitz et al., 1995). Notice that most of these free energies are for formation of dimers and are very close to the βpep-4 ΔG_D value of −7.3 kcal/mol. Moreover, thermodynamic stabilities of these dimeric peptide structures have also been associated with interfacial hydrophobic side-chain interactions which, in various combinations, impart greater or lesser stability.

As with coiled coils and four-helix bundles, exclusion of hydrophobic residues from polar solvent is the primary force that drives overall βpep-4 folding, and while fixed tertiary structure may contribute to a better defined and therefore a more stable subunit interface, the hydrophobic surface area of contact between D_{MG} monomer subunits is considerably greater than that between these dimer types in the tetramer. At the dimer–dimer (tetramer) interface, both hydrophobic contacts and hydrogen bonding between anti-parallel β-strands contribute to ΔG_T. Hydrophobic contact surface area, therefore, presumably dictates the larger free energy of monomer association regardless of internal flexibility in

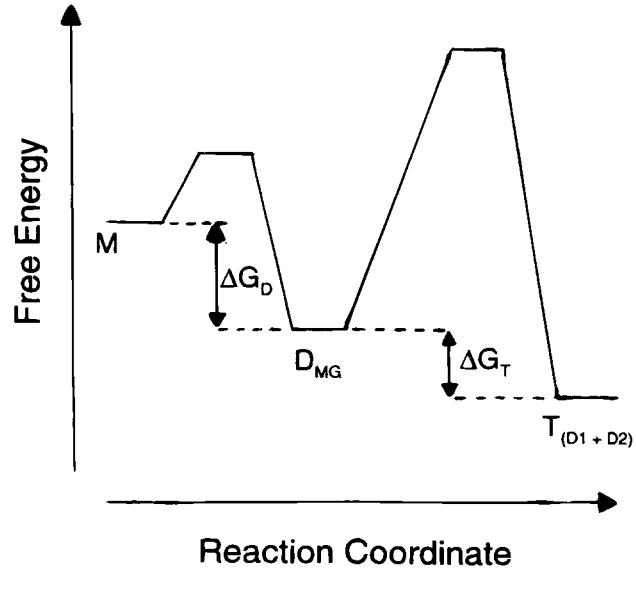

Fig. 7. Free energy level diagram for βpep-4 folding. A free energy level diagram is shown for the proposed βpep-4 folding pathway. The relative free energy is plotted on the vertical axis and a relative folding reaction coordinate is plotted on the horizontal axis.

D_{MG}. In fact, while considerable conformational entropy probably remains in D_{MG}, it is relatively reduced in $T_{(D1+D2)}$. Reduction in conformational entropy (internal flexibility) contributes to a more positive ΔG.

Figure 7 also shows activation energy barriers between D_{MG} and $T_{(D1+D2)}$ and between M and D_{MG}. The exchange rate between D_{MG} and M appears to be fast on the NMR chemical shift time scale (greater than 1,000 s^{-1}), because only one set of non-tetramer TOCSY cross-peaks could be discerned for individual amino acid spin systems when the βpep-4 concentration was reduced to where mostly dimer and monomer states were present. On the other hand, the D_{MG} to $T_{(D1+D2)}$ transition is slow on the NMR chemical shift time scale. This is indicated by the observation of individual sets of resonances in TOCSY contour plots for $T_{(D1+D2)}$ and lower oligomer states (primarily dimers) resonating more upfield. A slower exchange rate indicates a higher activation energy barrier as depicted in Figure 7 for the D_{MG} to $T_{(D1+D2)}$ transition.

The jump rate from $T_{(D1+D2)}$ to D_{MG} can be estimated from line width changes (Jardetsky & Roberts, 1981) as the population of folded tetramer decreases with decreasing peptide concentration. Downfield αH resonances are broader at lower concentrations where structured tetramer populations are less. Under the assumption that line width changes are due solely to the subunit exchange process, these data indicate that the exchange rate from the tetramer state is about 20 s^{-1} to 100 s^{-1} (depending on concentration), or that the lifetime of the compact tetramer is on the order of 10 ms to 50 ms. This time scale is similar to that observed for monomer–dimer–tetramer oligomer exchange in protein platelet factor-4 (Chen & Mayo, 1991).

βpep-4 β-sheet folding is thermodynamically linked with subunit association. Somehow on the reaction coordinate, D_{MG} makes the transition to a well-folded, β-sheet sandwich tetramer ($T_{(D1+D2)}$), which occurs slowly on the chemical shift time scale. This suggests that the inherent folding or conformational rearrangement process to well-folded tetramers falls on the order of about 100 ms. This is as fast as the folding of monomeric proteins where initial stages of folding occur on a time scale of less than about 5 ms and the final folding step to a well-structured state is rate limiting and occurs on a slower time. For example, native structure is formed in a few hundred ms in barstar (Nolting et al., 1997) and hen lysozyme (Radford et al., 1992), and in less than 20 ms in chymotrypsin inhibitor-2 (Jackson & Fersht, 1991) and less than 10 ms in ubiquitin (Briggs & Roder, 1992). With βpep-4, however, the folding process includes both dimer–dimer inter-molecular association and conformational re-shuffling to acheive the final folded state.

The mechanism by which this occurs is unknown. It may be that "molten globule-like" dimers (D_{MG}) first rapidly associate to form less structured tetramers, which then undergo a slower conformational transition to the well-folded tetramer state. The alternative is to consider that D_{MG} makes the transition to well-structured dimers, which then associate into tetramers. This later scenario is less likely because a relatively large population of D_{MG} is observed with no evidence for the presence of well-folded dimers. Moreover, from the unfolding side of the equilibrium, well-structured βpep-4 tetramers [$T_{(D1+D2)}$] dissociate into some initial dimer state that could remain well-structured for a period of time. Because a buildup of well-folded dimer is not observed, however, the rate of unfolding to D_{MG} must occur on a time scale that is faster than that for $T_{(D1+D2)}$ dissociation, i.e., faster than 1 to10 ms. In any event, the unfolding step from $T_{(D1+D2)}$ to D_{MG} and then to M is very rapid relative to the unfolding kinetics in small monomeric proteins. For example, barnase (Matouschek et al., 1989) has a half-life of several hundred seconds, while chymotrypsin inhibitor 2 (Jackson & Fersht, 1991) and Trp synthease α-subunit (Beasty et al., 1986) have half-lives greater than 1 h, and human lysozyme (Taniyama et al., 1992) has a half-life of several days. This fast unfolding step is but another way to view the relative instability of βpep-4 β-sheet structure outside the tetramer. Apparently hydrophobic side-chain interactions alone (at least in the context of the βpep-4 sandwich dimer) are not sufficient to maintain well-folded structure. Optimal side-chain packing is crucial to fold stability and compactness (Tanimura et al., 1994). Perhaps the unique structure in the tetramer is locked in when interfacial dimer–dimer β-strand hydrogen bonds fall into the appropriate register between subunits. This should occur in a correlated fashion with good side-chain packing of the sandwiched hydrophobics-residues. Behe et al. (1991) reported that hydrophobic interactions alone provide insufficient directionality and specificity for native-like folding. In βpep-4, the interfacial β-strand hydrogen bonds could direct the uniqueness of the fold.

βpep-4 folding at the quaternary level is in many ways analogous to folding on the tertiary level with small monomeric proteins. There, an unfolded (U) protein folds rapidly to a partially folded or perhaps intermediate state (I) (maybe a molten globule), which then undergoes a slower transition to the native (N) fully folded state. In our case, βpep-4 monomers have mostly unordered conformation, forming little β-sheet structure outside of higher oligomer states; molten globule-like dimers (D_{MG}) may serve as a model folding intermediate, which associates and then folds further in a rate-limiting step to form well-structured, in this case native, tetramers ($T_{(D1+D2)}$). The transition from D_{MG} to $T_{(D1+D2)}$ is particularly intriguing and mandates further study, which is currently underway.

Materials and methods

Peptide synthesis

The 33 residue peptide, βpep-4: SIQDLNVSMKLFRKQAKWKI IVKLNDGRELSLD, was synthesized on a Milligen Biosearch 9600 automated peptide synthesizer. The procedures used were based on Merrifield solid-phase synthesis utilizing Fmoc-BOP chemistry (Stewart & Young, 1984). After the sequence was obtained, the peptide support and side-chain protection groups were acid (trifluoroacetic acid and scavenger mixture) cleaved. Crude peptide was analyzed for purity on a Hewlett-Packard 1090M analytical HPLC using a reverse-phase C18 VyDac column. Peptide generally was about 90% pure. Further purification was done on a preparative reverse-phase HPLC C-18 column using an elution gradient of 0–60% acetonitrile with 0.1% trifluoroacetic acid in water. βpep-4 then was analyzed for amino acid composition on a Beckman 6300 amino acid analyzer by total hydrolysis of samples using 6 N HCl at 110 °C for 18–20 h. N-terminal sequencing confirmed peptide purity.

NMR measurements

For NMR measurements, freeze-dried peptide was dissolved either in D_2O or in H_2O/D_2O (9:1). Protein concentration normally was in the range of 1 to 5 mM. pH was adjusted by adding μL quantities of NaOD or DCl to the peptide sample. NMR spectra were acquired on a Varian Inova Unity Plus 600 spectrometer.

2D-Homonuclear magnetization transfer (HOHAHA) spectra, obtained by spin locking with a MLEV-17 sequence (Bax & Davis, 1985) with a mixing time of 60 ms, were used to identify spin systems. NOESY experiments (Jeener et al., 1979; Wider et al., 1984) were performed for conformational analysis. All 2D-NMR spectra were acquired in the TPPI (Marion & Wüthrich, 1983) or States (States et al., 1982; Marion et al., 1985) phase sensitive mode. The water resonance was suppressed by direct irradiation (0.8 s) at the water frequency during the relaxation delay between scans as well as during the mixing time in NOESY experiments. 2D-NMR spectra were collected as 256 to 400 t1 experiments, each with 1 k or 2 k complex data points over a spectral width of 6 kHz in both dimensions with the carrier placed on the water resonance. For HOHAHA and NOESY spectra, normally 16 and 64 scans, respectively, were time averaged per t1 experiment. Data were processed directly on the spectrometer or off line using FELIX (Molecular Simulations, Inc.) on an SGI workstation. Data sets were multiplied in both dimensions by a 30–60° shifted sine-bell function and zero-filled to 1 k in the t1 dimension prior to Fourier transformation.

Pulsed-field gradient NMR self-diffusion measurements

Pulsed field gradient (PFG) NMR self-diffusion measurements were acquired using a 5-mm triple-resonance probe equipped with an actively shielded z-gradient coil. The maximum magnitude of the gradient was calibrated by using the standard manufacturer's procedure and was found to be 60 G/cm, which is consistent with the value of 61 G/cm obtained from analysis of PFG data on water using its known diffusion constant (Mills, 1973). The linearity of the gradient was checked by performing diffusion measurements on water over different ranges of the gradient. The PFG longitudinal eddy-current delay pulse sequence (Gibbs & Johnson, 1991) was used for all self-diffusion measurements that were performed in D_2O over the temperature range 278 to 313 K. Peptide concentrations ranged from 0.05 to 20 mg/mL.

For unrestricted diffusion of a molecule in an isotropic liquid, the relative change in the PFG-NMR signal amplitude is related to the diffusion coefficient, D, by (Stejskal & Tanner, 1965):

$$R = \exp[-\gamma^2 g^2 \delta^2 D(\Delta - \delta/3)] \quad (3)$$

where γ is the gyromagnetic ratio of the observed nucleus; g and δ are the magnitude and duration of the magnetic field-gradient pulses, respectively, and Δ is the time between the gradient pulses. For these studies, experimental conditions were: $\delta = 4$ ms, $g = 1$ to 45 G/cm, $\Delta = 34.2$ ms, and the longitudinal eddy-current delay $T_e = 100$ μs. Each diffusion constant was determined from a series of 15 one-dimensional PFG spectra acquired using different g values. Experimental decay curves were approximated as single exponentials. Three upfield methyl and methylene resonances were used to derive average D values for each set of conditions.

PFG NMR self-diffusion measurements were also performed on globular proteins lysozyme, ribonuclease, and ubiquitin as standards. At 293 K, D values are 10.1×10^{-7} cm^2/s for lysozyme, 10.2×10^{-7} cm^2/s for ribonuclease, and 14.3×10^{-7} cm^2/s for ubiquitin. These D values agree reasonably well with those values in the literature: 10.6×10^{-7} cm^2/s for lysozyme (Dubin et al., 1971) obtained from light scattering by extrapolation to infinite dilution; 10.7×10^{-7} cm^2/s (Squire & Himmel, 1979) for ribonuclease also obtained from light scattering by extrapolation to infinite dilution, and 14.9×10^{-7} cm^2/s for ubiquitin (Altieri et al., 1995) obtained by using similar PFG NMR measurements. This relatively good agreement in diffusion coefficients indicates that the PFG longitudinal eddy-current delay-pulse sequence allows derivation of accurate diffusion constant values.

The Stokes-Einstein equation $D = k_B T/6\pi\eta R$ was used to relate D to the macromolecular radius, R, which in turn, is considered to be proportional to a power, a, of the apparent molecular weight, M_{app}. For solid spheres, R is proportional to $M_{app}^{1/3}$, while for random coils R is proportional to $M_{app}^{1/2}$ (Cantor & Schimmel, 1980). Typically $a = 1/3$ is used for compact globular proteins. In general, when comparing diffusion coefficients for two proteins, 1 and 2, of the same type (either both random coil or both compact) under the same conditions:

$$D_1/D_2 = (M_{2\,app}/M_{1\,app})^a. \quad (4)$$

Use of the Stokes-Einstein relationship has been derived specifically for a hard sphere. The actual molecular shape and the shape of the molecular oligomer are expected to affect the diffusion coefficient. The maximum change, for example, in D_{dimer} due to dimer geometry compared to D of a spherical molecule of equal volume would be about 5% (Teller et al., 1979).

Circular dichroism

Circular dichroic (CD) spectra were measured on a JASCO JA-710 automatic recording spectropolarimeter coupled with a data processor. Curves were recorded digitally and fed through the data processor for signal averaging and baseline subtraction. Spectra were recorded from 278 to 313 K in the presence of 10 mM potassium phosphate, over a 185 to 250 nm range using a 0.5 mm path-length, thermally jacketed quartz cuvette. Temperature was controlled by using a NesLab water bath. Peptide concentration was varied from 0.014 to 0.14 mM. The scan speed was 20 nm/min. Spectra were signal averaged eight times, and an equally signal-averaged solvent baseline was subtracted.

Acknowledgments

This work was supported by generous research grants from the Minnesota Medical Foundation and the Graduate School of the University of Minnesota. NMR experiments were performed at the University of Minnesota High Field-NMR Laboratory. Peptides were synthesized at the Microchemical Facility, Institute of Human Genetics, University of Minnesota. We are grateful to Dinesha S. Walek for her expertise in peptide synthesis.

References

Altieri AS, Hinton DP, Byrd RA. 1995. Association of biomolecular systems via pulsed field gradient NMR self-diffusion measurements. *J Am Chem Soc 117*:7566–7567.

Bax A, Davis DG. 1985. MLEV-17-based two-dimensional homonuclear magnetization transfer spectroscopy. *J Magn Reson 65*:355–360.

Beasty AM, Hurle MR, Manz JT, Stackhouse T, Onuffer JJ, Matthews CR. 1986. Effects of the F22L, E49M, G234D and G234K mutations on the folding and stability of the α-subunit of Trp synthase from *E. coli*. *Biochemistry 25*:2965–2974.

Behe MJ, Lattman EE, Rose GD. 1991. The protein-folding problem: The native fold determines packing, but does packing determine the native fold? *Proc Natl Acad Sci USA 88*:4195–4199.

Bierzynski A, Kim PS, Baldwin RL. 1982. A salt bridge stabilizes the helix formed by isolated C-peptide of RNase A. *Proc Natl Acad Sci USA 79*:2470–2474.

Blanco FJ, Jimenez MA, Herranz J, Rico M, Santoro J, Nieto JL. 1993. NMR evidence of a short linear peptide that folds into a β-hairpin in aqueous solution. *J Am Chem Soc 115*:5887–5888.

Briggs MS, Roder H. 1992. Early hydrogen-bonding event in the folding reaction of ubiquitin. *Proc Natl Acad Sci USA 89*:2017–2021.

Bryson JW, Betz SF, Lu HS, Suich DJ, Zhou HX, O'Neil KT, DeGrado WF. 1995. Protein design: A hierarchic approach. *Science 270*:935–941.

Cantor CR, Schimmel PR. 1980. *The behavior of biological macromolecules. Biophysical chemistry, part III.* New York: W.H. Freeman. pp 979–1039.

Chen MJ, Mayo KH. 1991. Human platelet factor-4 subunit association/dissociation thermodynamics and kinetics. *Biochemistry 30*:6402–6411.

de Alba E, Jimenez MA, Rico M, Nieto J. 1997. Conformational investigation of designed short linear peptides able to fold into β-hairpin structures in aqueous solution. *Folding Design 1*:133–144.

Dubin SB, Clark NA, Benedek GB. 1971. Measurement of the rotational diffusion coefficients of lysozyme in solution. *J Chem Phys 54*:5158–5165.

Gibbs SJ, Johnson CS. 1991. A PFG NMR experiment for accurate diffusion and flow studies in the presence of eddy currents. *J Magn Reson 93*:395–402.

Greenfield N, Fasman GD. 1969. Computed circular dichroism spectra for the evaluation of protein conformation. *Biochemistry 8*:4108–4116.

Harbury PB, Zhang T, Kim PS, Alber T. 1993. A switch between two-, three-, and four-stranded coiled coils in GCN4 leucine zipper mutants. *Science 262*:1401–1407.

Ilyina E, Roongta V, Mayo KH. 1997a. Designing water soluble β-sheet peptides with compact structure. *Technol Protein Chem VIII*. Forthcoming.

Ilyina E, Roongta V, Mayo KH. 1997b. NMR structure of a *de Novo* designed, peptide 33mer with two distinct, compact β-sheet folds. *Biochemistry 36*:5245–5250.

Jackson SE, Fersht AR. 1991. Folding of chymotrypsin inhibitor 2. Influence of proline isomerization on the folding kinetics and thermodynamic characterization of the transition state of folding. *Biochemistry 30*:10436–10443.

Jaenicke R. 1991. Protein folding: Local structures, domains, subunits, and assemblies. *Biochemistry 30*:3147–3161.

Jardetsky O, Roberts GCK. 1981. *NMR in molecular biology*. New York: Academic Press.

Jeener J, Meier B, Backman P, Ernst RR. 1979. Investigation of exchange processes by two-dimensional NMR spectroscopy. *J Chem Phys 71*:4546–4550.

Johnson WC Jr. 1990. Protein secondary structure and circular dichroism: A practical guide. *Proteins 7*:205–214.

Kaumaya PT, Berndt KD, Heidorn DB, Trewhella J, Kezdy FJ, Goldberg E. 1990. Synthesis and biophysical characterization of engineered topographic immunogenic determinants with alpha alpha topology. *Biochemistry 29*:13–23.

Lumb KJ, Carr CM, Kim PS. 1994. Subdomain folding of the coiled coil leucine zipper from the bZIP transcriptional activator GCN4. *Biochemistry 33*:7361–7367.

Marion D, Wüthrich K. 1983. Application of phase sensitive two-dimensional correlated spectroscopy (COSY) for measurements of ^{1}H-^{1}H spin-spin. *Biochem Biophys Res Commun 113*:967–975.

Marion D, Ikura M, Tschudin R, Bax A. 1985. Rapid recording of 2D NMR spectra without phase cycling. Application to the study of hydrogen exchange in proteins. *J Magn Reson 89*:393–399.

Matouschek A, Kellis JJ, Serrano L, Fersht AR. 1989. Mapping the transition state and pathway of protein folding by protein engineering. *Nature 340*:122–126.

Mayo KH, Ilyina E, Park H. 1996. A recipe for designing water-soluble, β-sheet-forming peptides. *Protein Sci 5*:1301–1315.

Mills R. 1973. Self-diffusion in normal and heavy water in the range of 1-45°. *J Phys Chem 77*:685–688.

Munson M, O'Brien R, Sturtevant JM, Regan L. 1994. Redesigning the hydrophobic core of a four-helix-bundle protein. *Protein Sci 3*:2015–2022.

Nolting B, Golbik R, Neira JL, Soler-Gonzalez AS, Schreiber G, Fersht AR. 1997. The folding pathway of a protein at high resolution from microseconds to seconds. *Proc Natl Acad Sci USA 94*:826–830.

Ptitsyn OB, Misotnov GV. 1991. In: Nall BT, Dill KA, eds. *Conformations and forces in protein folding*. Washington, DC: Amerucal Association for Advanced Science.

Quinn TP, Tweedy NB, Williams RW, Richardson JS, Richardson DC. 1994. Betadoublet: De novo design, synthesis and characterization of a beta-sandwich protein. *Proc Natl Acad Sci USA 91*:8747–8751.

Radford SE, Dobson CM, Evans PA. 1992. The folding of hen lysozyme involves partially structured intermediates and multiple pathways. *Nature 358*:302–307.

Rajarathnam K, Sykes BD, Kay CM, Dewald B, Geiser T, Baggiolini M, Clark-Lewis I. 1994. Neutrophil activation by monomeric interleukin-8. *Science 264*:90–92.

Rajarathnam K, Clark-Lewis I, Sykes BD. 1995. ^{1}H NMR solution structure of an active monomeric interleukin-8. *Biochemistry 34*:12983–12990.

Ramirez-Alvarado M, Blanco FJ, Serrano L. 1996. *De novo* design and structural characterization of a model β-hairpin peptide system. *Nat Struct Biol 3*:604–611.

Richardson JS, Richardson DC. 1989. The de novo design of protein structures. *Trends Biochem Sci 14*:304–309.

Richardson JS, Richardson DC, Tweedy NB, Gernert KM, Quinn TP, Hecht MH, Erickson BW, Yang Y, McClain RD, Donlan ME, Surles MC. 1992. Looking at proteins: Representations, folding, packing, and design. *Biophys J 63*:1185–1209.

Ross PD, Subramanian S. 1981. Thermodynamics of protein association reactions: Forces contributing to stability. *Biochemistry 20*:3096–3102.

Shoemaker KR, Kim PS, Brems DN, Marqusee S, York EJ, Chaiken IM, Baldwin RL. 1985. Nature of the charged-group effect on the stability of the C-peptide helix. *Proc Natl Acad Sci USA 82*:2349–2353.

Squire PG, Himmel ME. 1979. Hydrodynamics and protein hydration. *Arch Biochem Biophys 196*:165–167.

States DJ, Haberkorn RA, Ruben DJ. 1982. A two-dimensional nuclear Overhauser experiment with pure absorption phase in four quadrants. *J Magn Reson 48*:286–293.

Stewart JM, Young JD. 1984. *Solid phase peptide synthesis*, 2nd ed. Rockford, IL: Pierce Chemical Co. p 135.

Stejskal EO, Tanner JE. 1965. Spin diffusion measurements: Spin echoes in the presence of a time dependent field gradient. *J Chem Phys 42*:288–292.

Tanford C. 1981. *Physical chemistry of macromolecules*. New York: Wiley. pp 286–296.

Tanimura R, Kidera A, Nakamura H. 1994. Determinants of protein side-chain packing. *Protein Sci 3*:2358–2365.

Taniyama Y, Ogasahara K, Yutani K, Kikuchi M. 1992. Folding mechanism of mutant human lysozyme C77/95A with increased secretion efficiency in yeast. *J Biol Chem 267*:4619–4624.

Teller DC, Swanson E, de Haen C. 1979. The translational friction coefficient of proteins. *Methods Enzymol 61*:103–124.

Waterhous DV, Johnson WC. 1994. Importance of environment in determining secondary structure in proteins. *Biochemistry 33*:2121–2128.

Wider G, Macura S, Anil-Kumar, Ernst RR, Wüthrich K. 1984. Homonuclear two-dimensional 1H NMR of proteins. Experimental procedures. *J Magn Reson 56*:207–234.

Wishart DS, Sykes BD, Richards FM. 1992. The chemical shift index: A fast and simple method for the assignment of protein secondary structure through NMR spectroscopy. *Biochemistry 31*:1647–1651.

Wüthrich K. 1986. *NMR of proteins and nucleic acids*. New York: Wiley-Interscience.

Yan Y, Erickson BW. 1994. Engineering of betabellin 14D: Disulfide-induced folding of a β-sheet protein. *Protein Sci 3*:1069–1073.

Zitzewitz JA, Bilsel O, Luo J, Jones BE, Matthews CR. 1995. Probing the folding mechanism of a leucine zipper peptide by stopped-flow circular dichroism spectroscopy. *Biochemistry 34*:12812–12819.